Plasma treatment as a method for functionalising and improving dispersion of carbon nanotubes in epoxy resins

J. Williams · W. Broughton · T. Koukoulas ·
S. S. Rahatekar

Abstract This study reports on the results of plasma-treated carbon nanotubes (CNTs) in the presence of oxygen and ammonia which can be scaled up for relatively large quantities of nanomaterials. The plasma treatment has been shown to change the surface chemistry and energy as well as the morphology of the carbon nanotubes. X-ray photo-electron spectroscopy analysis shows increases in oxygen and nitrogen groups on the oxygen- and ammonia-treated CNTs, respectively. Titration of the enhanced oxygen plasma-treated CNTs reveals an increased presence of carboxylic acid groups at 2.97 wt% whilst bulk density decreases from 151 kg/m^3 for untreated carbon nanotubes to 76 kg/m^3 after the enhanced oxygen treatment. The free surface energy has also been shown to increase from 33.70 up to 53.72 mJ/m^2 determined using a capillary rise technique. The plasma-treated carbon nanotubes have been mixed in epoxy and have shown an improvement in dispersion, which was quantitatively evaluated using an optical coherence tomography (OCT) technique shown to be suitable for nanocomposite characterisation. This research has demonstrated that it is possible to surface functionalise large quantities of carbon nanotubes in a single process, and that this process improves the dispersion of the carbon nanotubes in epoxy.

J. Williams · S. S. Rahatekar (✉)
ACCIS, Department of Aerospace Engineering, University
of Bristol, Bristol BS8 1TR, UK
e-mail: Sameer.Rahatekar@Bristol.ac.uk

W. Broughton · T. Koukoulas
Materials Division, National Physical Laboratory,
Teddington TW11 OLW, UK
e-mail: Bill.Broughton@npl.co.uk

Introduction

Two major challenges exist in developing high performance polymer nanocomposites, namely achieving good dispersion and quantifying the quality of dispersion. Achieving good dispersion of CNTs in a polymer is often reported as being difficult [1–4]. Good dispersion is essential if the properties of CNTs are to be utilised to their full potential within a matrix material. Commercially available carbon nanotubes are inert, hydrophobic, and highly entangled and are therefore difficult to disperse in solvents and polymers.

The most common method for improving CNTs compatibility with a polymer matrix consists of extensive acid treatments [3–8] or the use of dispersing agents [9–12]. In the case of acid treatments typically the CNTs will undergo sonication in mixture of concentrated sulphuric and nitric acid, followed by a washing stage in sodium hydroxide. The CNTs are then filtered and dried. In general, the aim of this treatment is to introduce various functional groups such as carboxyl (–COOH) and hydroxyl (–OH) on the surface of CNTs, as these improve the solubility in common solvents and are compatible with epoxy resins. The addition of carboxyl groups also gives the potential for the CNTs to bond covalently with a polymer as well as offer substitution sites for other functional groups to be grafted on afterwards such as amines and esters [4]. The dispersant approach is less involved than the acid treatments as the dispersing agent is often mixed in situ with the polymer CNT solution. A common dispersion method uses a surfactant with a hydrophobic head that is attracted toward the CNT, whilst the hydrophilic tail associates with a solvent or polymer for dissolution, this creates a barrier stopping re-agglomeration of the CNTs [11, 13]. Although, the surfactants have been shown to improve dispersion in many

solvents and polymers [14–19] there is no associated molecular bonding between either the CNTs or the polymer. This reduces the mechanical-reinforcing potential of the CNTs within the polymer.

An alternative method for adding functional groups to CNTs and improve their compatibility is by plasma treatment. Plasma treatment is advantageous compared to acid treatments as it is a dry process and functionalisation can be done in one step. Current plasma processes reported in literature [20–22] only treat small quantities of material typically less than 1 g at a time, making these processes nonviable on a commercial scale. Here, we use a technology scale-up to potentially functionalise kilograms of CNTs in one process by plasma treatment. The work demonstrates that it is possible to control the degree of functionalisation and the chemical species by varying the plasma processing parameters, such as process gases, gas pressure, processing times, and plasma power; making it a versatile process, thus confirming previous observations reported [20].

Another difficulty in developing good quality nanocomposites is to quantify the dispersion of CNTs. A number of approaches have been proposed [23–25] for quantifying dispersions, including scanning electron microscopy techniques using computer algorithms to analyse particle distributions. These methods are useful, but obtaining SEM images is fairly time consuming requiring special sample preparation and locating a representative reference area.

In this report, an optical method that has previously been presented [26] is used to quantify the dispersion by a static light scattering technique, optical coherence tomography. This technique has been used to quantify the dispersion of the cured epoxy–CNT composite. This nondestructive technique has the advantage of optically depth probing the material without requiring special sample preparation, making it a quick process suitable for industrial use. The plasma surface treatments used on the CNTs to improve their dispersion in epoxy and the quantitative method to measure the dispersion presented in this report, provides an extremely useful tool for scientists and engineers to produce high performance nanocomposites.

Experimental

Epoxy system

The epoxy matrix used for this study was Prime 20LV manufactured by Gurit Ltd. The epoxy is based on diglycidyl ether of bisphenol F (DGEBF) blended with reactive diluents to reduce the viscosity. The slow amine-based hardener was used to increase handling time. The epoxy system is designed for infusion processes due to its low viscosity. This made injection and the removal of air bubbles easier with the addition of carbon nanotubes.

Plasma treatment of carbon nanotubes

The carbon nanotubes used throughout this study were Bayertubes C150P, a multiwalled carbon nanotube powder produced by Bayer Materials Science by a catalytic chemical vapour deposition method. The carbon nanotubes have been plasma treated by Haydale Ltd using their lab scale plasma reactor equipment especially designed for handling relatively large quantities of nano material typically 25 g. The aim of these treatments was to make the carbon nanotubes more hydrophilic by adding polar groups to aid dispersion [4]. Three different plasma treatments were carried out for comparison with an untreated sample. Table 1 summarises the carbon nanotubes used in this report and their naming convention used throughout.

The enhanced treatment differs from the standard treatment by increasing the processing time, plasma power, and gas pressure compared to the standard treatment, the aim for the enhanced oxygen treatment was to increase the carboxylic content for its reactive properties. An enhanced ammonia treatment was not pursued as the initial treatment damaged the vacuum pump seals (the seals have subsequently been redesigned to facilitate ammonia treatment options).

Carbon nanotube epoxy dispersion process

Carbon nanotube powders at 1 wt% were dispersed in Prime 20LV epoxy resin using a Silverson L5M-A Lab Mixer, with a square hole, high shear mixing head for a standard running time of 90 min at 5000 rpm. Once the resin and carbon nanotube powders were mixed, the Prime 20LV slow hardener was added to a ratio of 100 parts resin to 26 parts hardener by weight as recommended by the manufacturer. This was followed by intense mixing for 5 min before a degassing stage of 15 min. Using a syringe to draw the mixture from the mixing pot, the solution was injected into the mould. The silicon mould contained 25 mm square pockets for creating samples used for the OCT measurements. Once cast the epoxy was cured at 50 °C for 16 h as recommended by the manufacturer.

Table 1 Plasma treatments assessed

Name	Gas treatment	Remarks
C150P-AR	None	As received material
C150P-O	Oxygen	Standard treatment
C150P-NH$_3$	Ammonia	Standard treatment
C150P-EO	Oxygen	Enhanced treatment

Characterisation and measurement techniques

X-ray photoelectron spectroscopy

An initial X-ray photoelectron spectroscopy (XPS) survey was carried out on the carbon nanotubes to determine their surface composition after plasma treatment, using a VG Escalab MkII using un-monochromated Al K alpha X-rays at 1486.6 eV. To reveal the subsurface degree of functionalisation, subsequent XPS analysis was achieved by grinding the CNT powder and argon ion sputtering using a Kratos minibeam-I ion-source on a Kratos Axis Ultra-DLD system. The argon ion source operated at 4 kV, with an argon gas pressure of 1×10^{-6} Torr. The sputtering was performed by rastering over a 5 mm^2 wide area for 2 min. The sample target current as measured by the Vision software was 6.5 μA. Spectra were acquired over an area of approximately 300×700 μm for the Kratos Axis and 2×2 mm on the Escalab MkII . Data analysis was performed using CasaXPS using sensitivity factors provided by the manufacturer.

Titration

Titration has been used to determine the quantity of acid groups such as carboxylic acid present on the carbon nanotubes after plasma treatment. The measurement has been made using a Metrohm Titrando 809 potentiometric titrating device. The functionalised carbon nanotubes are reacted with an excess of aqueous sodium hydroxide and the unreacted excess aqueous sodium hydroxide is then titrated with aqueous hydrochloric acid (HCl). The titration procedure is as follows; 1 g of carbon nanotubes are added to 110 mL of distilled water and exactly 10 mL of 1M aqueous sodium hydroxide NaOH solution is added by the titration device and stirred for 5 min, followed by the addition of 1M hydrochloric acid. The potential change and the quantity of hydrochloric acid required to neutralize the solution is then recorded by the titration device. A blind value (BV) using the same procedure is calculated in the same way without the addition of the carbon nanotubes as a means of calibration. Using the equivalent point, the acid number (AN) mass in milligrams of potassium hydroxide required to neutralise the solution is calculated as follows.

$$AN(mg) = \frac{(BV(mL) - HCl(mL)) \times M(KOH)(g/mol)}{Mass\ of\ CNTs(g)}$$

(1)

The weight percent of carboxylic acid groups present has been calculated as follows:-

$$wt\% = \frac{AN \times M(COOH)(g/mol)}{1000 \times M(KOH)(g/mol) \times Mass\ of\ CNTs(g)}$$

(2)

where M(KOH) and M(COOH) values of 56.1 and 45 g/mol relate to the molar mass of potassium hydroxide and carboxylic acid, respectively.

Capillary rise

Capillary rise has been used to determine the surface free energy of the processed carbon nanotube powders. A Sigma 700 Tensiometer with a 12 mm diameter powder sample holder, equipped with a spring-loaded cap has been used for repeatable packing. Consistent packing has been shown to be essential for dependable results [27]. The procedure is based on previously published work [27–30] as follows:

Grade 1 Whatman® filter paper is placed at the bottom of the powder module. 100 mg of the CNT powder is poured into the powder holder. The tube is then tapped in a repeatable manner to settle the powder and the spring-loaded cap is applied to compress the powder. The powder holder is then hooked on to the tensiometers electronic balance. The probe liquid is placed below on a motorised stage in a beaker. Once ready, the experiment is started and the beaker is raised slowly (1 mm/min) until it comes into contact with the powder holder. Once the tensiometer has detected this, it then measures mass increase with respect to time at 0.1 second intervals. Once the change in mass has plateaued the experiment can be stopped.

Hexane was used as the reference experiment due to its low surface tension and it is assumed to perfectly wet any solid at an angle of 0°, hence $\cos\theta = 1$ in the modified Washburn equation (3) [27, 30, 31] leaving one unknown constant, K. The material constant K is calculated from the gradient of the steepest linear section of the mass^2 versus time plot, this was done using the tenisometer's Attension software linear regression function. Using other polar and non-polar probe liquids (Details, Table 2) and taking further gradients of the steepest linear section of the mass^2 versus time plots, the contact angles of different probe liquids were calculated by manipulating the same Eq. (3). The probe liquids were reagent grades purchased from Sigma-Aldrich. The experiments were repeated five times for each sample in a controlled laboratory environment at 20 °C. where W is the mass, t the time, K the material constant, ρ the liquid density, $\cos\theta$ the contact angle, η the

Table 2 Characteristics of probe liquids at 20 °C [27, 32]

Liquid	ρ (kg/m^3)	η (mPa·s)	γ_L (mN/m)	γ_l^d (mN/m)	γ_l^p (mN/m)
Hexane	0.659	0.318	18.42	18.42	0.00
Toluene	0.867	0.590	28.52	28.52	0.00
Water	1.002	0.998	72.60	21.60	51.00

viscosity, and γ the surface energy (solids)/tensions (liquids) with subscripts s, solid; l, liquid; and superscripts d, dispersive; p, polar.

$$\frac{\Delta W^2}{\Delta t} = \frac{K\rho^2\gamma_1 cos\theta}{\eta} \tag{3}$$

$$\gamma_s^d = \frac{\gamma_1^d(1 + cos\theta)^2}{4} \tag{4}$$

$$\gamma_1(1 + cos\theta) = 2(\sqrt{\gamma_1^p\gamma_s^p} + \sqrt{\gamma_1^d\gamma_s^d}) \tag{5}$$

The total free surface energy γ_s of the solid has been calculated in two parts using procedure outlined by [33]. Firstly using the simple Fowkes equation (4) [34], the dispersive part of the surface energy must be calculated using a non polar liquid (Toluene). This leaves one unknown in the Fowkes equation (5), γ_s^p which can be calculated by using a polar liquid (distilled water). The total free surface energy of the solid is the sum of the dispersive and polar parts as per Eq. (6).

$$\gamma_s = \gamma_s^d + \gamma_s^p \tag{6}$$

Electron microscopy

Scanning electron microscopy (SEM) images were taken by a JEOL JSM 6330F ultra high vacuum SEM at an acceleration voltage of 10 kV. The nanotube powder samples were taken without sputtering. Samples for the fracture surface images were silver sputtered.

OCT measurement

OCT has been used to provide high resolution three-dimensional (3-D) imaging (<7.5 μm lateral and <10 μm axial) of the sub-surface structure of the nanocomposite samples. The technique, which is based on low coherence interferometry (LCI) works to a depth of 2–3 mm. It is worth noting that depth of penetration decreases with increasing particle loading. The dominant contrast mechanism utilised in LCI is variation in refractive index that gives rise to an increase in direct backscattering of incoming photons [26]. OCT enables 3-D imaging by acquiring individual two-dimensional (2-D) or information resulting from the refractive index boundaries within the sample. A distinct difference in refractive index exists between the nanoparticles, which act as light scatterers, and the surrounding polymer matrix. Depth scan information is extracted from a recording of the intensity of the back scattered light. In this case, Fourier domain optical coherence tomography (FD-OCT) was utilised; a Michelson Diagnostics EX1301 multi-beam OCT microscope was used for this purpose, operating in a swept frequency mode with a centre wavelength of 1305 nm and a bandwidth of

150 nm. FD-OCT translates wave-domain information into the time-domain to provide information on the materials structure. The system consists of four laser beams focused at different depths over a depth of focus of 0.25 mm each, providing a total focal range of 1 mm. Although MWCNTs may be 10–40 nm in diameter, nanotube length is typically 1–2 μm, which is of sufficient length to interact with the interrogating laser beam.

FD-OCT was used to generate a series of B-scan images (4 μm spatial spacing between scans (layers)) that were converted to C-scan images using ImageJ software. During the measurements, it is possible to end up with noise contributions from artefacts due to high reflections from top and bottom surfaces of the sample. These artefacts reduce gradually as the penetration depth increases at the cost of decreasing signal-to-noise (S/N) ratio. By applying wavelet analysis for each layer it is possible to reduce the effect of these artefacts. Wavelet analysis is a mathematical tool used to extract localised temporal (or spatial) and frequency information (i.e., signal processing) from audio signals and video images. Each OCT image separated into a set of orthogonal (horizontal and vertical) and diagonal wavelets that facilitate image analysis. Efficacy of this approach is dependent on the quality of the specimen. The specimen's top and bottom surfaces should be polished and parallel in order to obtain the best S/N ratio and to avoid curvature effects on the optical wavefront. In reality, specimen surfaces tend to be irregular. The approach adopted was to select a sub-surface layer slightly below the top surface free of any surface features due to reflections and representative of the bulk material. The layer depth selected will depend on the quality of the specimen and the ability of the laser beam to penetrate the material. For MWCNT-based polymer nanocomposites (PNCs), the penetration depth is often limited to less than 250 μm. A C-scan image (slice) at a depth of ≈ 20 μm, or greater was used for this study. Sampling depths in excess of 20 μm was required to minimise (or eliminate) the effect of surface reflections. A liquid with a refractive index of 1.57 was applied to the surface in order to reduce surface reflections.

The analysis was performed in MATLAB. Each C-scan image was decomposed into first order horizontal, vertical, and diagonal wavelets. These were in turn segmented into 16×16 2-D cluster arrays (i.e., 256 clusters in total) and the average of the standard deviations for each cluster was calculated, producing a surface of specific roughness for the horizontal, vertical, and diagonal wavelets. The average value of the standard deviations for the three wavelets for each cluster was then calculated and the average of all these values was assigned to the spatial layer to provide a measure of the degree of particle dispersion. For low levels of dispersion, the standard deviation will be larger

compared to well-dispersed samples, thus providing a metric for quantifying dispersion.

Results and discussions

Plasma treatment analysis

The XPS results are shown in two parts in Table 3. Firstly the results after plasma treatment presputtering show the plasma treatments have changed the surface composition compared to the untreated, C150P-AR CNTs. A similar increase in oxygen content is shown for the oxygen-treated C150P-O/-EO CNTs indicating the saturation point for adding additional oxygen has already been reached by this process. The additional oxygen content indicates an increase in oxygen containing groups, such as carbonyl, hydroxyl, and carboxyl being grafted to the surface [20]. Whilst the C150P-NH$_3$ tubes show nitrogen present corresponding to amine, nitrile, amide, and oxime groups on the surface of the carbon nanotubes [20]. The oxygen present on the C150P-AR tubes is thought to be due to the imperfect nature of the CNTs allowing oxygen to bond to the surface when they are exposed to the atmosphere after the production process.

The postsputtering experiments were designed to expose the core of the CNT powders for analysis, so as to study the difference between the surface and bulk functionalisation. In all cases the results show a reduction in oxygen present and also nitrogen for the C150P-NH$_3$ CNTs. This demonstrates that the plasma treatments are more affective on the surface of the CNTs. The trace quantities of argon present can be attributed to the argon ion sputtering process.

Titration

The titration results in Table 4 shows that the extended oxygen treatment C150P-EO had the largest increase in its recorded acid number compared to any other sample. The increase in acid number relates to an increase in the quantity of carboxyl functional groups being present on

the carbon nanotubes. Although, the XPS results for the C150P-O and C150-EO are very similar in terms of quantity of oxygen present the acid number is not. This suggests the standard oxygen treatment favoured groups such as carbonyl, whilst the enhanced treatment favoured carboxyl groups which is in accordance with previously reported observations [20].

Capillary rise surface energy measurements

The free surface energy results from the capillary rise experiments are shown in Table 5. In general the treated carbon nanotube powders show an increase in their free surface energy, with the enhanced oxygen-treated powder showing the largest increase. These results show that treating the carbon nanotubes in this way will improve their wettability, and hence their compatibility with matrix materials such as epoxies. This matches observations made with the increased difficulty of mixing the C150P-AR CNTs as compared to the plasma-treated CNTs.

Of interest to note is large contact angle of almost 90° for the C150P-AR powder with water is close to the capillary rise method's limit of applicability and signalling the hydrophobic nature of these untreated carbon nanotubes. For the treated CNTs smaller contact angles have been calculated with water. This can be attributed to the additional polar groups such as hydroxyl, carboxyl, and amines that have been added from the plasma treatment processes which will be miscible with polar liquids such as water. Due to the lower surface tension of toluene, the overall contact angles observed are lower than compared to water

Table 4 Titration results

Material	Acid number	Carboxylic acid (wt%)
C150P-AR	0	0
C150P-O	3	0.24
C150P-NH$_3$	N/A	N/A
C150P-EO	37	2.97

Table 3 XPS survey results

Material	XPS survey data (atomic %)						
	XPS results presputter			XPS results postsputter			
	Carbon	Oxygen	Nitrogen	Carbon	Oxygen	Nitrogen	Argon
C150P-AR	96	4	0	–	–	–	–
C150P-O	92.2	7.8	0	97.47	2.08	0	0.45
C150P-NH$_3$	94	3.8	2.2	96.48	2.88	0.14	0.5
C150P-EO	92.6	7.4	0	97.01	2.52	0	0.47

Table 5 Surface energy results

Material	Water cont' $\angle\theta°$	Toluene cont' $\angle\theta°$	γ_s^d (mJ/m²)	γ_s^p (mJ/m²)	γ_s (mJ/m²)
C150P-AR	89.72	67.92	13.49 ± 0.87	20.21 ± 0.19	33.70 ± 1.06
C150P-O	81.02	37.83	22.82 ± 0.78	24.60 ± 3.42	47.42 ± 4.20
C150P-NH$_3$	79.51	41.19	21.88 ± 2.31	28.68 ± 3.74	50.57 ± 6.05
C150P-EO	76.81	23.83	26.12 ± 0.97	27.60 ± 2.07	53.72 ± 3.04

which would be expected. There is also a similar trend to water in that treated materials display lower contact angles with toluene resulting in higher dispersive components of their free surface energy.

SEM particle analysis and bulk density

The SEM images in Fig. 1 indicate that the entangled CNT particle size is greatly reduced after the plasma treatment process. The close-up SEM images show the entanglement of the carbon nanotubes within the agglomerated particles. Along with the reduced particle sizes, the enhanced oxygen treated agglomerates (d) are much more uniform compared to the others. It is also possible to observe individual tubes appearing to break free from the cluster which was not observed on any other sample.

It was also observed that the plasma treatment reduces the apparent bulk density of the material shown visually in Fig. 2 and shown in Table 6. This effect is most noticeable on the enhanced oxygen treatment, being roughly half the density of the unmodified material. This is an interesting result as treatments such as ball milling of CNTs are reported to reduce the agglomerate size as observed in this study but increase the apparent density [35–37].

Fracture surfaces

Fracture surface images have been taken of the nano composites as a qualitative measure of the dispersion of the carbon nanotubes within the epoxy. The brighter patches that can be seen in the images are clusters of nanotubes. Figure 3a of the untreated nanotubes shows the largest nanotube

(a) As received

(b) Oxygen treated

(c) Ammonia treated

(d) Enhanced oxygen treated
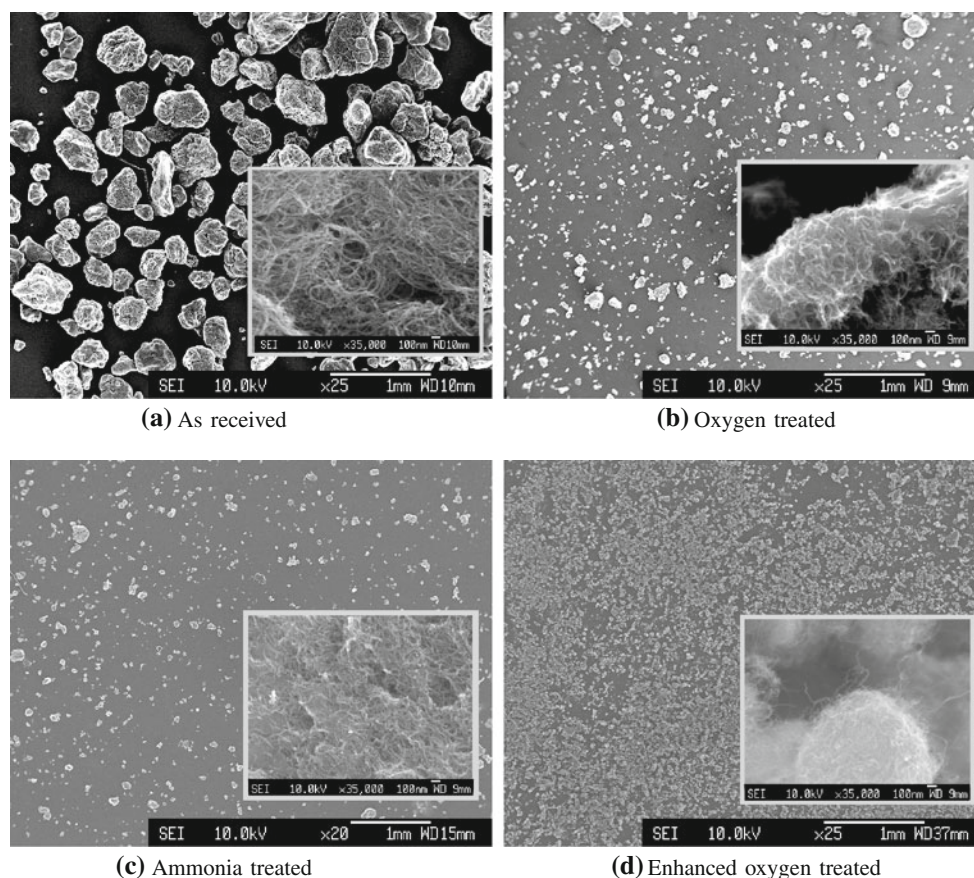
Fig. 1 SEM images of carbon nanotube powder; **a** As received, **b** Oxygen-, **c** Ammonia-, and (**d**) Enhanced oxygen-treated
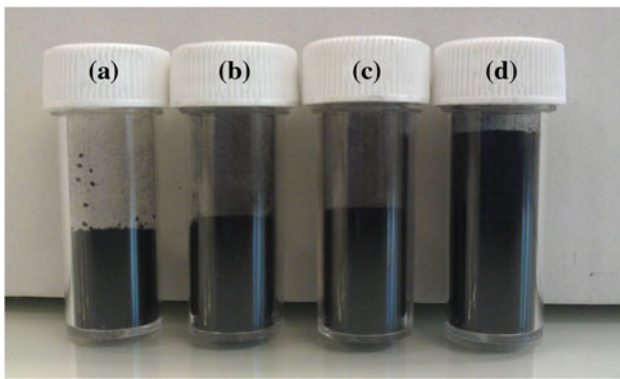
Fig. 2 Change in bulk density 0.4 g of CNTs in each: **a** CP150P-AR, **b** CP150P-O, **c** CP150P-NH$_3$, **d** CP150P-EO

Table 6 Bulk density measurements

Material	Bulk density kg/m^3
C150P-AR	151
C150P-O	131
C150P-NH$_3$	120
C150P-EO	76

clusters of all the samples, reflecting what is observed from its powder form. The oxygen and ammonia-treated carbon nanotube specimens Fig. 3b, c are still not particularly well dispersed as the carbon nanotubes still appear in patches but the presence of the larger agglomerates are gone. The fracture surface of the enhanced oxygen sample Fig. 3d has not fractured smoothly like the others. The rougher surface makes it difficult to distinguish between the nanotube patches and the raised edges which too appear bright in the SEM image. What can be declared however is the fracture surface appears more uniform, and a reduction of easily identifiable nanotube clusters is seen, suggesting an improvement in dispersion. The change in the fracture surface from smooth to rough indicates an increase in energy is required to fracture this nanocomposite compared to the others, suggesting a reinforcing affect.

Optical coherence tomography results

The surface roughness (average standard deviations) measurements obtained for the four different treatments using OCT, shown in Table 7, indicate that the plasma treatments
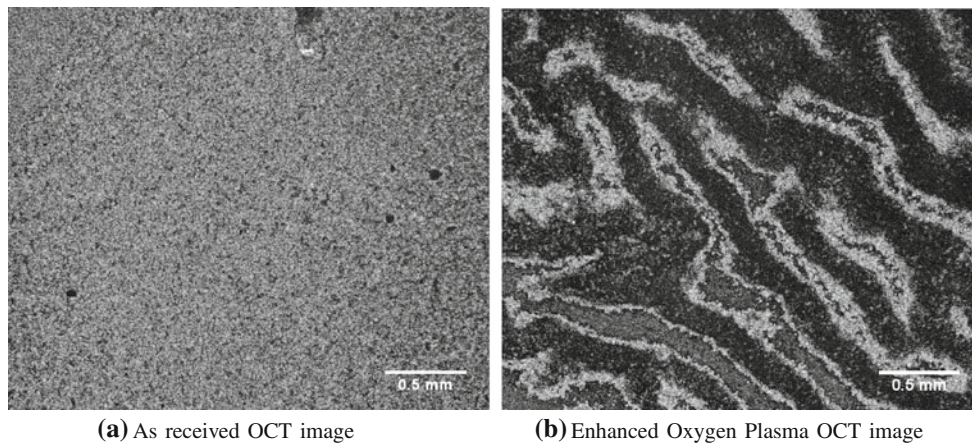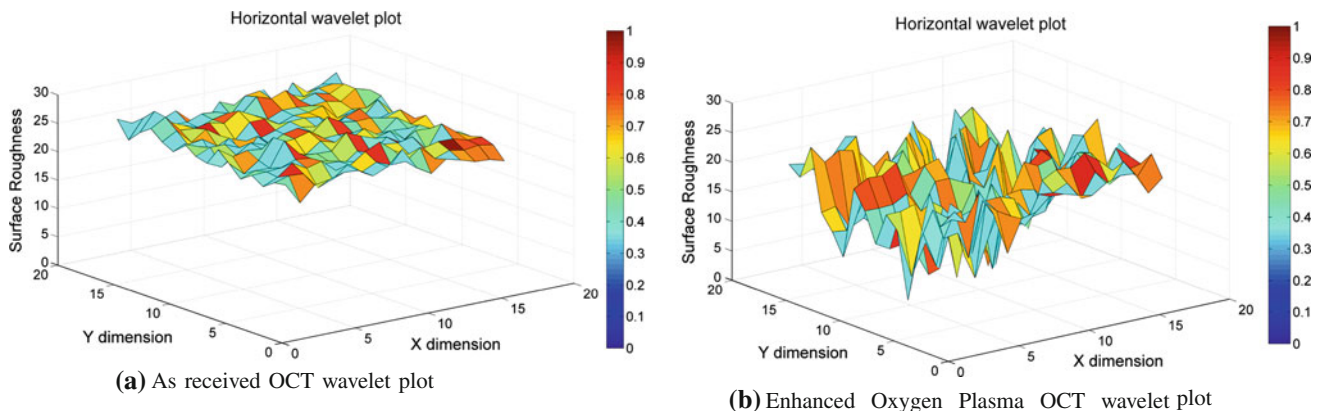

(a) As received

(b) Oxygen treated

(c) Ammonia treated

(d) Enhanced oxygen treated
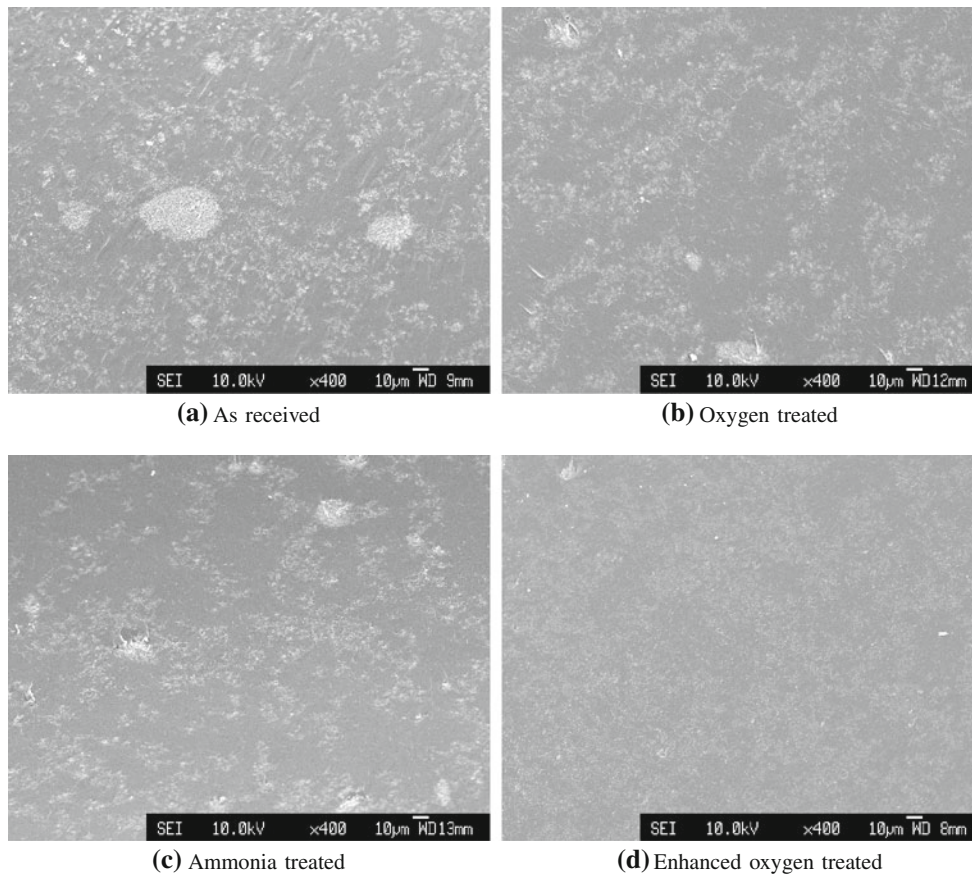
Fig. 3 SEM fracture surfaces images: **a** As received, **b** Oxygen-, **c** Ammonia-, and **d** Enhanced oxygen-treated

Table 7 OCT results

Material	OCT surface roughness
C150P-AR	26.34 ± 0.92
C150P-O	24.89 ± 1.50
C150P-NH$_3$	24.87 ± 1.06
C150P-EO	20.15 ± 4.87

result in improved levels of dispersion (increased uniformity) and that the enhanced oxygen treatment performs the best. This suggests that the reduction in bulk density, particle size, and increase in surface energy produced by the plasma treatment has a positive affect on the measured dispersion. Previous research [7] suggests that oxygen and ammonia surface treatments can add mutual electrostatic repulsion charges to the surface of the CNTs, which give the CNTs the potential to overcome the binding van der Waals forces and aid dispersion. In the case of the treatments considered in this study, it is thought to be a secondary effect compared to the reduced agglomerate size.

An interesting point arises by comparing the OCT surface roughness between the untreated (worst case) and enhanced oxygen (best case) treatments. The average standard deviation is, as explained and expected, higher for the former case and lower for the latter one, thus indicating better dispersion for the enhanced oxygen treatment in agreement with the results produced in this study. However, the bandwidth of the deviation (scatter) is lower for the untreated and higher for the enhanced treatment. This means that there are areas of high dispersion throughout the sample, but due to thermodynamic variations within the composite, there appears to be a pattern of well-dispersed regions. Figure 4 shows typical OCT C-scan images for the untreated and oxygen plasma-treated PNC materials and their corresponding horizontal wavelet (surface roughness) plots, which are shown in Fig. 5. The SEM images presented in Fig. 3 are approximately an order of magnitude smaller in scale compared to the OCT; showing a high degree of dispersion that agrees with the OCT data on a smaller localised scale.

(a) As received OCT image **(b)** Enhanced Oxygen Plasma OCT image

Fig. 4 OCT images of as received (**a**) and oxygen plasma treated (**b**) epoxy nanocomposites

(a) As received OCT wavelet plot **(b)** Enhanced Oxygen Plasma OCT wavelet plot

Fig. 5 As received and enhanced oxygen plasma OCT wavelet plots

Conclusions

This study has shown it is possible to treat relatively large quantities of carbon nanotubes by plasma in a single process. The resulting particles are shown to be much finer and the XPS and titration results have shown this process can add surface chemical groups to the nanotubes. The plasma treatments have been shown to mainly affect the surface of the CNT powders. Titration is a relatively quick and cheap process compared to XPS analysis and has shown that the enhanced oxygen treatment increases the acid content present by an order of magnitude compared to the standard treatment. Capillary rise has shown increases in free surface energy of the CNT powders, meaning the treated CNTs will wet better and be more easily miscible with a solvent or polymer compared to untreated material. It has been shown from the optical coherence tomography data and supported by the visual observations of the fracture surfaces, that the plasma treatments have improved the dispersion of the carbon nanotubes. The plasma-treated carbon nanotubes also have the added functional groups associated with them, which could potentially allow them to covalently bond with the epoxy matrix giving potential to improve the resulting mechanical properties. This study shows a useful means of improving the dispersion of highly entangled commercial carbon nanotubes through plasma treatment that can improve the quality of manufactured nanocomposites.

References

1. Gojny FH, Wichmann MH, Fiedler B, Schulte K (2005) Compos Sci Technol 65(1516):2300. doi:10.1016/j.compscitech.2005.04.021
2. Wang S, Liang Z, Liu T, Wang B, Zhang C (2006) Nanotechnology 17(6):1551. doi:10.1088/0957-4484/17/6/003
3. Zhu J, Kim J, Peng H, Margrave JL, Khabashesku VN, Barrera EV (2003) Nano Lett 3(8):1107. doi:10.1021/nl0342489
4. Ma PC, Siddiqui NA, Marom G, Kim JK (2010) Compos Part A 41(10):1345. doi:10.1016/j.compositesa.2010.07.003
5. Kim SD, Kim JW, Im JS, Kim YH, Lee YS (2007) J Fluorine Chem 128(1):60. doi:10.1016/j.jfluchem.2006.10.010
6. Kim YJ, Shin TS, Choi HD, Kwon JH, Chung YC, Yoon HG (2005) Carbon 43(1):23. doi:10.1016/j.carbon.2004.08.015
7. Hirsch A (2002) Angew Chem Int Ed 41(11):1853. doi:10.1002/1521-3773(20020603)41:111853::AID-ANIE18533.0.CO;2-N
8. Liu H, Cheng G, Zheng R, Zhao Y, Liang C (2005) J Mol Catal A 230(12):17. doi:10.1016/j.molcata.2004.12.003
9. Tkalya EE, Ghislandi M, de ~ With G, Koning CE (2012) Curr Opin Colloid Interface Sci 17(4): 225. doi:10.1016/j.cocis.2012.03.001
10. Kim KH, Jo WH (2008) Compos Sci Technol 68(9):2120. doi:10.1016/j.compscitech.2008.03.008
11. Loos M, Yang J, Feke D, Manas-Zloczower I (2012) Compos Sci Technol 72(4):482. doi:10.1016/j.compscitech.2011.11.034
12. Haggenmueller R, Rahatekar SS, Fagan JA, Chun J, Becker ML, Naik RR, Krauss T, Carlson L, Kadla JF, Trulove PC, Fox DF, DeLong HC, Fang Z, Kelley SO, Gilman JW (2008) Langmuir 24(9):5070. doi:http://pubs.acs.org/doi/abs/10.1021/la703008r. PMID:18442227
13. Wallace EJ, Sansom MSP (2009) Nanotechnology 20(4):045101. doi:10.1088/0957-4484/20/4/045101
14. Gong X, Liu J, Baskaran S, Voise RD, Young JS (2000) Chem Mater 12(4):1049. doi:10.1021/cm9906396
15. Moore VC, Strano MS, Haroz EH, Hauge RH, Smalley RE, Schmidt J, Talmon Y (2003) Nano Lett 3(10):1379. doi:10.1021/nl034524j
16. Krause B, Petzold G, Pegel S, Potschke P (2009) Carbon 47(3):602. doi:10.1016/j.carbon.2008.10.040
17. Vaisman L, Wagner HD, Marom G (2006) Adv Colloid Interface Sci 128–130:37. doi:10.1016/j.cis.2006.11.007
18. Rastogi R, Kaushal R, Tripathi S, Sharma AL, Kaur I, Bharadwaj LM (2008) J Colloid Interface Sci 328(2):421. doi:10.1016/j.jcis.2008.09.015
19. Wang H, Zhou W, Ho DL, Winey KI, Fischer JE, Glinka CJ, Hobbie EK (2004) Nano Lett 4(9):1789. doi:10.1021/nl048969z
20. Felten A, Bittencourt C, Pireaux JJ, Lier GV, Charlier JC (2005) J Appl Phys 98(7):074308. doi:10.1063/1.2071455
21. Ruelle B, Peeterbroeck S, Gouttebaron R, Godfroid T, Monteverde F, Dauchot JP, Alexandre M, Hecq M, Dubois P (2007) J Mater Chem 17:157. doi:10.1039/B613581C
22. Valentini L, Puglia D, Armentano I, Kenny J (2005) Chem Phys Lett 403(46):385. doi:10.1016/j.cplett.2005.01.042
23. Grasley ZC, Yazdanbakhsh A (2011) Compos Part A 42(12):2043. doi:10.1016/j.compositesa.2011.09.011
24. Tyson BM, Al-Rub RKA, Yazdanbakhsh A, Grasley Z (2011) Compos Part B 42(6):1395. doi:10.1016/j.compositesb.2011.05.020
25. Sul IH, Youn JR, Song YS (2011) Carbon 49(4):1473. doi:10.1016/j.carbon.2010.12.017
26. Koukoulas T, Broughton WR, Tedaldi M, Theobald PD (2011) Opt Meas Syst Indus Insp VII. doi:10.1117/12.889190
27. Siebold A, Walliser A, Nardin M, Oppliger M, Schultz J (1997) J Colloid Interface Sci 186(1):60. doi:10.1006/jcis.1996.4640
28. Shen Q, Mezgebe M, Li F, Dong JQ (2011) Colloids Surf A 390(13):212. doi:10.1016/j.colsurfa.2011.09.030
29. Mezgebe M, Shen Q, Zhang JY, Zhao YW (2012) Colloids Surf A 403(0):25. doi:10.1016/j.colsurfa.2012.03.045
30. Jackson P, Hunt J, Doherty P, Cannon A, Gilson P (2004) J Mater Sci: Mater Med 15:507. doi:10.1023/B:JMSM.0000021129.60818.ca
31. Washburn EW (1921) Phys Rev 17:273. doi:http://link.aps.org/doi/10.1103/PhysRev.17.273
32. Timmermans J (1950) In: Physico chemical constants of pure organic compounds. Elsevier, New York
33. Zenkiewicz M (2007) J Achiev Mater Manuf Eng 24:137
34. Fowkes FM (1964) Indus Eng Chem 56(12):40. doi:http://pubs.acs.org/doi/abs/10.1021/ie50660a008
35. Kukovecz A, Kanyo T, Konya Z, Kiricsi I (2005) Carbon 43(5):994. doi:10.1016/j.carbon.2004.11.030
36. Kim Y, Hayashi T, Fukai Y, Endo M, Yanagisawa T, Dresselhaus M (2002) Chem Phys Lett 355(34):279. doi:10.1016/S0009-2614(02)00248-8
37. Zapata-Massot C, Bolay NL (2008) Chem Eng Proc 47(8):1350. doi:10.1016/j.cep.2007.05.001